

****FULL TITLE****

*ASP Conference Series, Vol. **VOLUME**, **YEAR OF PUBLICATION***

****NAMES OF EDITORS****

Outflows from Massive Stars

John Bally

*Department of Astrophysical and Planetary Sciences,
University of Colorado, Boulder, CO 80389, USA.*

Abstract. The properties of outflows powered by massive stars are reviewed with an emphasis on the nearest examples, Orion and Cepheus-A.

1. Introduction

Outflows are ubiquitous in star forming regions. They provide observable constraints on the accretion histories and dynamical evolution of forming stars, and represent a major channel for self-regulation of star formation and feedback. Our understanding of outflow phenomena has grown dramatically as new wavelength regimes, higher resolution, and greater sensitivity produced a flood of new observations. However, observers have mostly focused on relatively nearby outflows that are powered by low- to moderate-mass YSOs (for reviews see Reipurth & Bally 2001; and the articles in Reipurth, Jewitt, & Keil 2007). Thus, the study of outflows from massive stars is still in its infancy.

Massive stars are rare and tend to form in high pressure, opaque cores that produce clusters. Therefore, massive star outflows tend to be distant, highly obscured, and located in crowded and confused environments. Furthermore, their swept-up molecular shells and cavities can be rapidly obliterated by UV radiation and winds as the massive stars reach the main sequence. The nearest massive star outflow emerges from the highly obscured BNKL complex in the OMC1 cloud core located immediately behind the Orion Nebula at a distance of about 400 to 430 pc (Menten et al 2007; Hirota et al 2007; Sandstrom et al. 2007). The next best studied massive-star outflow is associated with Cepheus-A located about 725 pc from the Sun. Following a few general comments about massive star outflows, the OMC1 and Cep-A flows will be discussed in some detail.

2. Outflows from Massive Young Stellar Objects (MYSOs)

MYSOs can be identified by their large IR luminosities, the presence of maser emission, ultra- or hyper-compact HII regions, massive hot cores, high velocity wings in mm or sub-mm emission lines, the presence of shock-excited species such as H₂ and [FeII], and, if the obscuration is sufficiently low, Herbig-Haro (HH) objects. MYSOs can be subdivided according to their luminosity. Intermediate mass objects that reach peak luminosities of $L < 10^3 L_{\odot}$ become Herbig Ae or Be stars with masses of 2 to 8 M_{\odot} and are massive analogs to T Tauri stars. They produce copious soft-UV, but little or no ionization of hydrogen.

MYSOs with peak luminosities $L = 10^3$ to about $3 \times 10^4 L_\odot$ become early B or late O stars that can rapidly photo-ionize their environments. Most MYSOs (including Cep A) are in these two categories; they tend to have outflows that are scaled-up versions of outflows from low-mass stars. Their outflows tend to be highly collimated, contain multiple internal working surfaces, have mass-loss rates of 10^{-5} to *few* $\times 10^{-4} M_\odot \text{ yr}^{-1}$, momentum injection rates around 10^{-4} to $10^{-2} M_\odot \text{ yr}^{-1} \text{ km s}^{-1}$, and mechanical luminosities of 10^{-1} to $10^2 L_\odot$ that increase approximately linearly with stellar luminosity. MYSOs that approach or exceed $L \approx 10^5 L_\odot$ become the exceedingly rare, most massive early O-type stars. Their outflows are frequently poorly collimated with a morphology resembling an explosion; examples include the OMC1 / BNKL outflow in Orion and G34.26+0.15.

Beuther and Shepherd (2005) proposed an evolutionary scheme for massive YSOs. As the most massive stars accumulate their mass, they increase their luminosity and pass through each of the luminosity classes above. MYSOs with luminosities indicating spectral type B or later tend to have highly collimated outflows. By the time such stars have acquired a mass of about $10 M_\odot$, they will have reached the main sequence and their UV radiation fields will heat and ionize their immediate surroundings. MYSOs with luminosities of early B or late O stars tend to be surrounded by hyper- or ultra-compact HII regions and hot molecular cores with complex chemistry and their outflows tend to be less-well collimated. The most luminous MYSOs sometimes have very poorly collimated flows. However, except for Orion, these luminous objects tend to be studied with poor spatial resolution. Thus, their morphology may not be fully resolved in available data; some may be powered by many individual YSOs. Some ultra-massive outflows such as DR21 are likely to be powered by the collective effects of entire clusters of stars.

In luminous sources, UV radiation and line-driven winds can make major contributions to the momentum and energy injected into surrounding gas. When large reservoirs of dense, molecular gas survive in the immediate vicinity of a massive star or cluster, Lyman continuum can produce a compact HII region that vents into the lower density ISM. For certain geometries such as thick torii, or for a massive star embedded in a cylindrical cavity within a dense cloud, the ionization fronts will be confined by recombinations to a value comparable to the radius of the cavity. Thermal expansion of the high pressure, photo-ionized plasma ablating from the walls of the cavity close to the star, will drive a flow along the axis of the cavity. The plasma can sometimes flow through a recombination front at about the sound speed in ionized gas, recombine, and cool to form a hypersonic flow of HI. A quasi-static flow can be established as photo-ablation from the walls of the reservoir replenishes the lost plasma. Thus, the HII region remains confined and does not evolve on a dynamical time, but can effectively fuel a powerful, radiation driven outflow. Such an ionizing radiation driven model may explain the energetics of the most massive outflows such as the $200 M_\odot$ Mon R2 outflows and the $3,000 M_\odot$ DR 21 HI outflow (Russell et al. 1992).

Massive stars tend to form in clustered environments where many YSOs power outflows simultaneously and where the gas pressure and turbulent energy density can be very large compared to lower-mass star forming regions. Figure

1 illustrates mm-wave molecular emission from the outflow complex emerging from the cluster associated with IRAS 05358+3543 located about 2 kpc from the Sun in the Auriga star forming clouds (Beuther et al. 2002). At least five distinct flows can be seen. The $2.12\ \mu\text{m}$ near-IR emission line of H_2 traces shock-excited molecular gas. Several additional outflows are revealed by this tracer (Figure 2). Some outflows from massive stars show evidence for large changes in the orientation of the outflow axis on a time-scale comparable to the outflow dynamical age. Examples include IRAS 20126+4104, and Cep-A. While C-symmetric bends in outflows are generally an indication of relative motion between the star and surrounding medium (e.g. Bally et al. 2006), point symmetry (S- or Z-shaped outflows) are generally an indication of a precessing outflow.

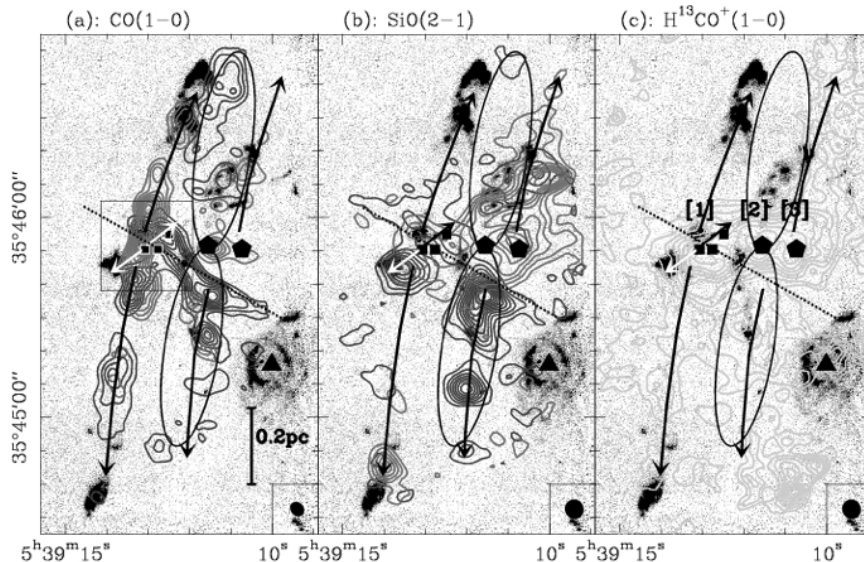


Figure 1. Multiple outflows bursting from the cluster associated with IRAS 05358+3543 (Beuther et al. 2002).

3. The Cepheus A Outflow

The Cep A star forming complex contains the second nearest region of massive star formation, next to the Orion complex. Located at a distance of 725 pc (Blaauw et al. 1959; Crawford & Barnes 1970), the Cep OB3 association contains a 20 by 60 pc molecular cloud that contains six localized peaks of CO emission designated Cepheus A through F (Sargent 1977, 1979). Cep A contains dense molecular clumps (Torrelles et al. 1993), molecular outflows (Rodriguez et al. 1980, Narayanan & Walker 1996), H_2O and OH masers (Cohen et al. 1984), hyper-compact H II regions (Hughes & Wouterloot 1984), variable radio

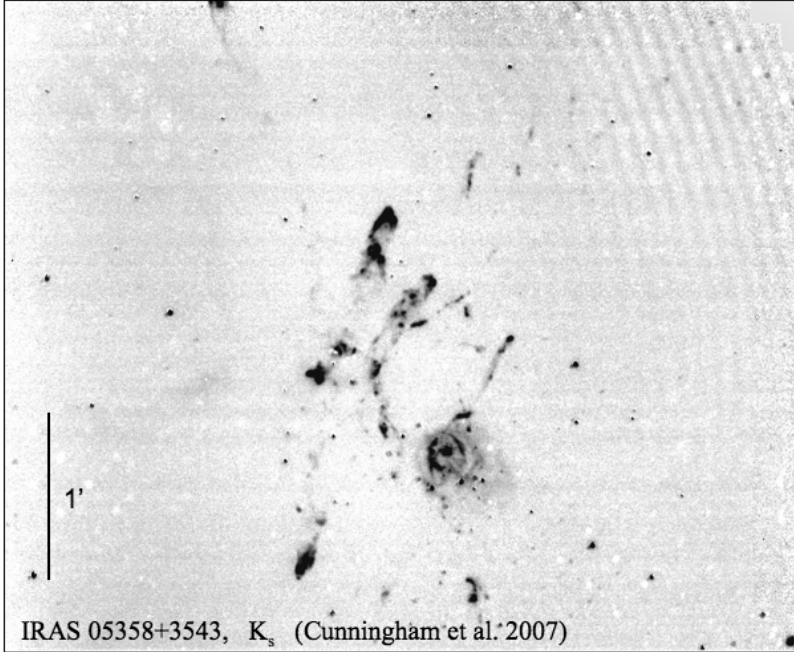


Figure 2. Multiple jets and additional outflows emerging from IRAS 05358+3543 and the associated young cluster as revealed by a $2.12\ \mu\text{m}$, continuum subtracted narrow-band image obtained with the near-IR camera NICFPS on the Apache Point Observatory 3.5 m telescope using 0.5% pass-band filters.

continuum sources (Garay et al. 1996), Herbig-Haro objects (Hartigan et al. 1986), bright shock-excited H_2 emission (Hartigan et al. 2000), a cluster of far-infrared sources with a luminosity of $2.5 \times 10^4 L_\odot$ (Koppelaar et al. 1979), and a cluster of Class I and Class II YSOs (Gutermuth et al. 2005). The bulk of the luminosity arises from radio sources HW2 and HW3c (Hughes & Wouterloot 1984) that are associated with bright H_2O masers.

Rodriguez et al. (1980) found a massive bipolar molecular outflow aligned primarily east-west. Single dish CO maps with $15''$ resolution (Bally & Lane 1990; Torrelles et al. 1993; Narayanan & Walker 1996) show that the flow is complex with a second redshifted peak west of the core, and with additional components aligned northeast-southwest. The inner part of the flow is blueshifted east and redshifted west of the radio source HW2. The additional redshifted component appears $6'$ west of HW2, bends to the northwest, and can be traced up to $12'$ from the Cep A core. The central $2'$ region contains high velocity (HV) as well as more compact extremely high velocity (EHV) CO components with a radial velocities ranging from -50 to $70\ \text{km s}^{-1}$ relative to the CO centroid. The axis of the EHV outflow is rotated roughly 40° clockwise relative to the HV outflow on the plane of the sky. The smaller extent together with the higher velocity suggests that the EHV flow traces a younger outflow component. Several self-absorption dips follow trends seen in the low-velocity line wings, with regions east of HW2 blueshifted and west of HW2 redshifted. Thus cooler,

self-absorbing gas traces the low-velocity bipolar outflow, rather than stationary gas surrounding the outflow. At low velocities, there are additional blue- and redshifted components centered on HW2 that are oriented northeast–southwest.

The Cep-A outflow complex contains several Herbig-Haro objects, including the extremely bright HH 168 located about $90''$ due west of HW2, and several fainter bow shocks located to the east (Hartigan, Morse, & Bally 2000). Fainter HH objects (HH 169 and 174) are located in the eastern, blueshifted lobe. Near-IR images show an extremely bright reflection nebula centered on HW2 with an illumination cone that opens towards the northeast. The $2.12\ \mu\text{m}$ H_2 line (Figure 3) exhibits a complex, filamentary structure.

3.1. Bipolar outflow from HW3c: HH 168 and its Counterflow

A series of bright arcs and bow shocks located 1 to $3'$ west of HW2 are associated with HH 168. The axes of symmetry of most of these shocks indicate a point of origin about $20''$ to $30''$ south of HW2. The luminous IR, maser, and radio source HW3c lies near this axis. A dim, $40''$ diameter bow shock is located on this axis about $2'$ east of HW3c, directly opposite HH 168. This feature and the visual-wavelength part of HH 168 are symmetrically placed about HW3c. Thus, HW3c is likely to be the source of these shocks and the associated CO outflow components. High-resolution cm-wavelength VLA observations (Garay et al 1996) reveal a chain of radio sources approximately aligned with the axis of this flow, and may either trace an ionized jet, or the interface between a jet and surrounding dense cloud material. Faint arcs of emission about $1'$ north of HH 168 trace the edges of a globule that contains an embedded, low-luminosity star. This emission is likely to be excited by UV radiation from the Cep OB3 association and is thus probably fluorescent in nature.

3.2. A pulsed, precessing Outflow from HW2?

The blueshifted, eastern lobe of the Cep-A outflow contains four distinct chains of H_2 emission radiating away from the immediate vicinity of HW2, each of which terminates in well-formed bow shocks. The axes of these chains, defined by lines connecting HW2 to the bow shocks at the eastern and north-eastern ends of the chains, shift systematically clockwise from nearly east–west to northeast–southwest. The longest chain, which terminates at HH 174, has a position angle measured from north to east of $\text{PA} \sim 95^\circ$. The second chain, which terminates at the eastern component of HH 169, has $\text{PA} \sim 80^\circ$. The third chain terminates at the western component of HH 169, has $\text{PA} \sim 65^\circ$. The fourth chain ends in a bright but compact H_2 bow at $\text{PA} \sim 55^\circ$. The current orientation of the HW2 radio jet is $\text{PA} \sim 45^\circ$. The chains of H_2 knots get progressively shorter with decreasing PA. This remarkable progression may be an indication that HW2 powers a pulsed and precessing jet.

A rough dynamical age for each chain can be estimated by dividing the length of each chain by the velocity of its tip. The radial velocities of the HH objects located at the ends of the first three chains are low ($V < 60\ \text{km s}^{-1}$), indicating that they most likely are moving close to the plane of the sky. Fabry-Perot imaging of the H_2 emission (Hirart et al. 2004) also indicate low, but chaotic radial velocities. On the other hand, excitation of the visual wavelength $\text{H}\alpha$ and $[\text{SII}]$ emission of the eastern HH objects and comparison with the speeds

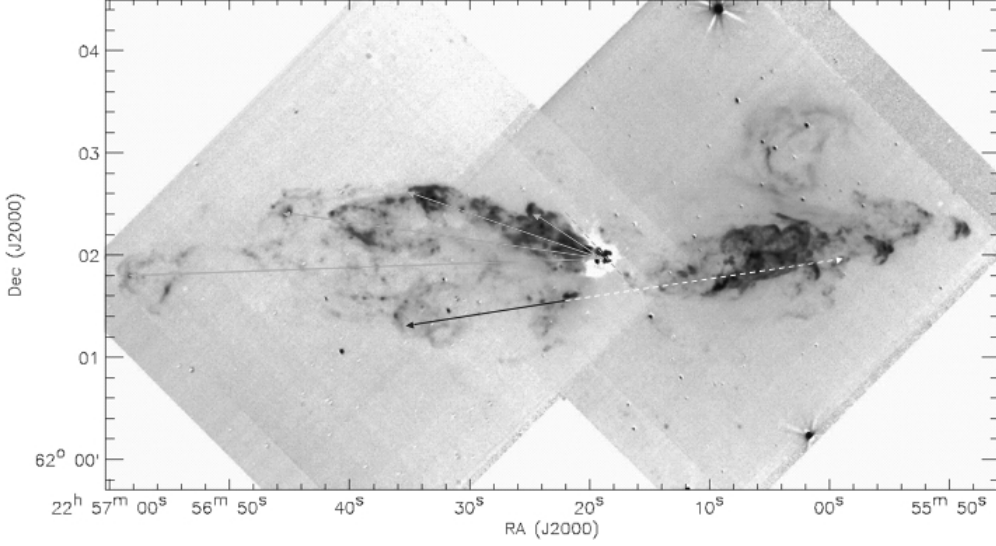


Figure 3. Continuum subtracted near-IR $2.12 \mu\text{m}$ emission from shock-excited H_2 in the Cep-A outflow complex. As discussed in the text, HW2 (located at the base of the 4 grey arrows inside the white patch near the middle of the image) appears to drive a pulsed, precessing jet whose orientation changes may be driven by forced precession induced by a companion star in an eccentric, non-coplanar orbit. The various suspected ejection directions are indicated by the light gray lines. The oldest (east-facing) ejection appears to power HH 174 located at the eastern edge of the image. The next two ejections may be responsible for HH 169 located near the northern boundary of the eastern outflow lobe. The current orientation of the radio jet emerging from HW2 is at position angle (PA) = 45° (northeast-southwest; dashed grey line). The bright objects HH 168 (dashed white line) west of the core, and the H_2 bow (near the tip of the solid black line) may be powered by HW3c located due south of HW2 along the dashed white line. From Cunningham (2006).

of other HH objects located at similar distances from their sources, indicate that shock speeds of order 100 km s^{-1} are not unreasonable. Using this speed, the dynamical ages of the four eastern H_2 chains are 10200, 7300, 4400, and 2100 years, respectively, indicating that an eruption / ejection event occurs approximately every 2,200. Furthermore, the presence of the HW2 radio jet indicates that there is currently an eruption underway.

Moeckel & Bally (2006, 2007a, b) use SPH simulations to show that in a dense proto-cluster, massive stars surrounded by circumstellar disks have a relatively high probability of capturing a passing cluster member because the disk makes such encounters dissipative. While such capture processes are relatively unimportant for Solar mass stars, they can be very important for massive ones due to their relatively much larger gravitational radii. Generally, binaries formed by such a capture process will have secondaries that move in eccentric and highly inclined orbits with respect to the plane of the disk or rotation axis of the primary. The motion of a companion on an eccentric and inclined orbit can drive forced precession of the disk. In contrast, multiples formed from disk

or core fragmentation tend to be move in co-planar orbits which do not result in precesing disks. Furthermore, the periastron passage of the companion can result in major disk perturbations that can result in episodes of mass accretion from the inner disk onto the primary.

Moeckel & Bally (2007a) modeled encounters between a $20 M_{\odot}$ star with a $2 M_{\odot}$, 500 AU disk and impactors of varying masses, periastron, and inclination angles. Cunningham, Moeckel, & Bally (2008) scaled those simulations to a mass similar to HW2, a $15 M_{\odot}$ primary with a 350 AU, $1.5 M_{\odot}$ disk. Disks were modeled using 1.28×10^5 particles, and followed through 5 encounters with the captured secondary. The mass of the impactor was chosen to be $5 M_{\odot}$ because a fairly massive companion is needed to torque the disk through $\sim 10^{\circ}$ during a periastron passage. The SPH simulations show that massive partners are more likely to be captured than low mass ones. Disks were modeled using $\sim 1.28 \times 10^5$ particles, and followed through 5 encounters. These models show that a capture formed binary with a secondary having about 1/3 of the mass of the primary, orbiting in a 2,000 year orbit can cause a massive disk to precess by about the amount observed in Cep A.

4. The Orion OMC1 Outflow

The BN/KL complex contains a remarkable, wide opening-angle (> 2 radian) outflow traced by molecules such as CO and NH_3 that exhibit broad ($> 100 \text{ km s}^{-1}$) emission lines (Kwan & Scoville 1976; Wiseman & Ho 1996) and high-velocity OH, H_2O , and SiO maser emission (Genzel et al. 1981; Greenhill et al. 1998). Hundreds of individual bow shocks are seen in the near-infrared wavelength emission lines of [FeII] and H_2 (Kaifu 2000; Figure 4). A few of these shocks protrude from the molecular cloud and can be seen at visual wavelengths. The morphology suggests an explosion; proper motions of visual and near-infrared features indicate a common age of about 10^3 years or less for many features (Doi et al. 2002; Figure 5). The outflow contains about $8 M_{\odot}$ of accelerated gas with a median velocity of about 19 km s^{-1} and maximum speeds in excess of 400 km s^{-1} . By one estimate, the current lower bound on the momentum and kinetic energy content are about $160 M_{\odot} \text{ km s}^{-1}$ and 4×10^{46} ergs, respectively (Snell et al. 1983). Other estimates indicate an outflow kinetic energy as high as 4×10^{47} ergs (Kaifu et al. 2000). The OMC1 core has a bolometric luminosity estimated to be about $10^5 L_{\odot}$ (Gezari, Beckman, & Werner 1998), indicating that the outflow region must contain one or more massive stars.

Multi-epoch radio-frequency images show that the three brightest radio-emitting stars in OMC1, sources BN, I, and n, have proper motions (motions in the plane of the sky) of 26, 15, and 24 km s^{-1} away from a region less than 500 AU in diameter from which they were ejected about 500 years ago (Rodriguez et al. 2005; Gomez et al. 2005). Apparently, a non-hierarchical multiple star system containing at least 4 massive members experienced a dynamical interaction resulting either in the formation of a tight binary or possibly a stellar merger (Bally & Zinnecker 2005) whose (negative) gravitational binding energy ejected these stars from the OMC1 core. With estimated stellar masses of 10, 20, and $10 M_{\odot}$ for BN, I, and n respectively, the kinetic energy of the stars is 2×10^{47} ergs (Rodriguez, et al., 2005; Gomez et al. 2005). Thus, the total energy required

to eject the stars and drive the OMC1 outflow is about 10^{48} ergs. This energy must be generated by the infall of two or more stars into a deeper gravitational potential well. Assuming that source I is a binary containing two $10 M_{\odot}$ stars, its members must be separated by less than 11 AU, the orbital period must be shorter than 7 years, and the perihelion velocity of the stars must be at least 70 km s^{-1} . This stellar ejection expelled a total of about $50 M_{\odot}$ of stars and gas from the OMC1 core.

The point of origin of the ejected stars is located at the center of the BN/KL outflow about $4''$ (2000 AU) northwest of the present location of source I. The stars and outflow have similar ages and kinetic energies. Therefore, it is likely that the outflow and dynamical ejection of the stars have a related origin. During the formation of a tightly bound, massive binary in a small-N interaction, gravitational potential energy can be transferred to the other stars, but their motion has little effect on the surrounding gas.

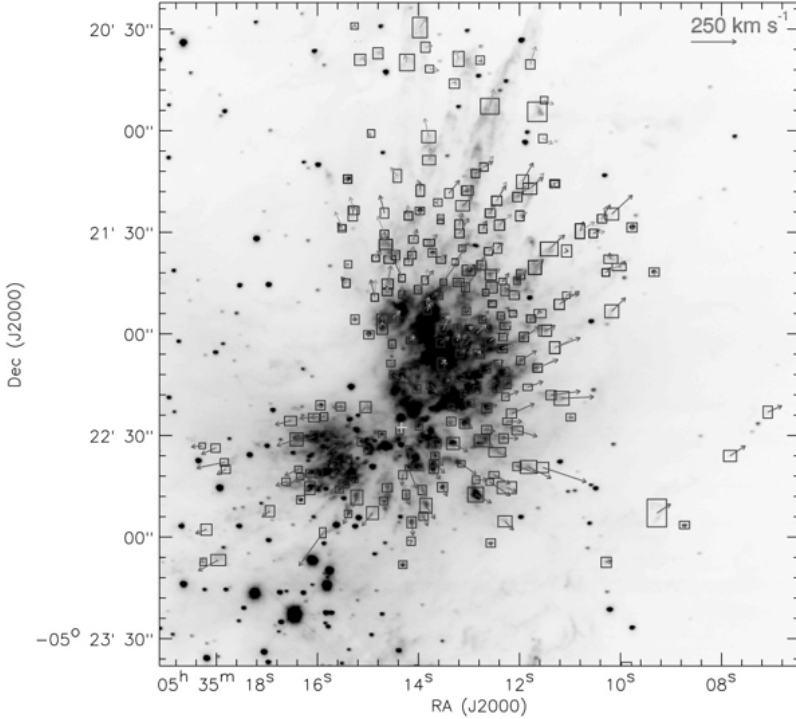


Figure 4. The OMC1 outflow as observed in the $2.12 \mu\text{m}$ lines of H_2 using a 0.5% passband filter and the NICFPS camera on the Apache Point Observatory 3.5 meter telescope. Vectors show showing proper motion measured by comparing this image, taken in 2005, with the Allen & Burton (1993) discovery images and the Kaifu et al. (2000) image obtained with the Subaru 8.4 meter. Taken from Cunningham (2006).

4.1. The Magnetic Bomb

We propose that over the last 10^5 years, the birth and subsequent orbital motion of a non-hierarchical cluster of 4 or 5 massive stars in OMC1 led to the

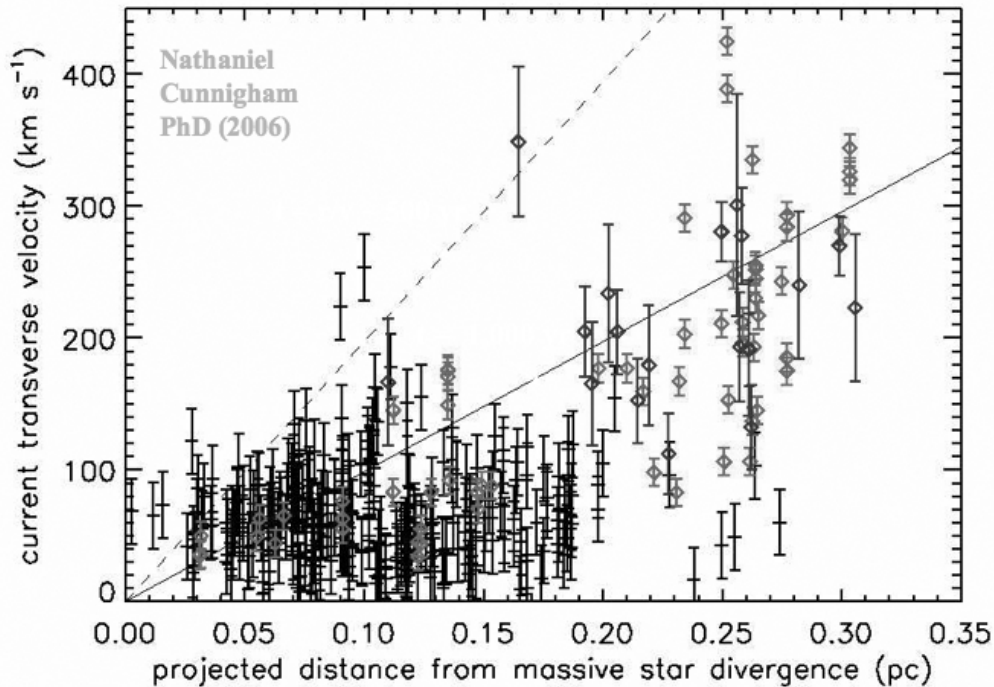


Figure 5. Proper motions in the OMC1 outflow as observed in the $2.12 \mu\text{m}$ lines of H_2 (black) and at visual wavelength using narrow-band filters on the Hubble Space Telescope (grey). From Doi et al. (2002) and Cunningham (2006).

amplification of the ambient magnetic field until it stored about 10^{48} ergs of magnetic energy in the volume inhabited by the cluster. About 500 years ago, this cluster decayed into a hierarchical configuration consisting of a short-period run-away binary and two high-velocity stars. The removal of about $50 M_\odot$ left the circum-cluster gas in the region severely magnetically over-pressured. The sudden release of magnetic energy, in effect a ‘magnetic bomb’ (Matt, Frank, & Blackman 2004, 2006; Lynden-Bell 1996; Wheeler, Meier, & Wilson 2002), may have been responsible for launching the OMC1 outflow. The following paragraphs explain in more detail how this scenario may work.

As a cloud core collapses, interstellar magnetic fields will be dragged in with the gas that eventually forms a small group of massive stars. The resulting magnetic field strength grows as the field lines are compressed, wound, and stretched and is thought to scale as n_H^α , where n_H is the number density of the gas and α is about 0.5. For the estimated density of the hot core in Orion of $n_H \approx 10^7 \text{ cm}^{-3}$, this scaling implies $\langle B \rangle = 10$ milli-gauss. Zeeman measurement of the magnetic fields using OH masers in BN/KL imply magnetic fields as high as 15 milli-gauss spread across a roughly 30 arcsecond diameter region ($\sim 10^4 \text{ AU}$; Cohen et al. 2006). Similar results are found in other massive star forming cores such as Cepheus A (Bartkiewicz et al. 2005; Vlemmings 2006).

Thus, we assume that the magnetic field had a strength of 10 milli-gauss when a small group of massive stars started to form in OMC1 about 10^5 years ago.

If the star formation efficiency that led to the formation of a $40 M_\odot$ sub-cluster of massive stars in OMC1 is 40%, the initial mass of gas involved must have been about $100 M_\odot$. Accretion of gas from the OMC1 core and dynamical friction enabled the forming stars to migrate deep into the cluster potential well to produce a compact, non-hierarchical multiple star system. This gravitational contraction of gas and stars ultimately provides the energy for the launched gas and ejected stars, so it is convenient to express the gravitational energy as E_{48} , the energy required to power the OMC1 outflow and run-away stars in units of 10^{48} ergs. The final radius is then given by $r \approx GM^2/E = 178M_{100}^2 E_{48}^{-1}$ AU, where M_{100} is the enclosed mass (in units of $100 M_\odot$). We postulate that during the last 10^5 years, 4 or more stars formed a non-hierarchical system with a characteristic diameter of order 200 to 400 AU and a total mass of about $40 M_\odot$. Such non-hierarchical multiple star systems are dynamically unstable and typically decay within 10 to 100 dynamical times (Sterzik & Durisen 1998).

The orbital motion of the protostars in their mutual gravitational potential well and the orbital motion of gas in individual circumstellar disks will each contribute to the amplification of the magnetic field by means of a shear dynamo. In linear winding, the final field strength B is related to the initial field as $B = 2\pi N B_0$, where N is the number of windings of the field lines. When equipartition is reached, $B^2 \approx 8\pi\rho c_s^2$, where $\rho = \mu m_H n_H = 3M/4\pi r^3$ is the gas density, and c_s is the effective sound speed including turbulent motions. The maximum field strength is obtained when the effective sound speed is similar to the gravitational escape speed. Thus, $c_s^2 \approx GM/r$ where M is the mass enclosed inside radius r . The spatially averaged equipartition value of B is then given by $B \approx (6/r^3)^{1/2} = (6G)^{1/2} M/r^2 \approx 42 E_{48}^{1/2} r_{100}^{-3/2}$ (gauss) where r_{100} is in units of 100 AU. The orbital time scale about $100 M_\odot$ of gas and stars at this radius is about 100 years, so to obtain the maximum average field of order 40 gauss from an initial field of $B_0 = 10$ milli-gauss with linear growth requires about 700 orbits or less than 0.7×10^5 years, comparable to the typical time required to accrete a star.

Efficient field amplification of B in the potential well requires a sufficient degree of ionization to couple the magnetic field to the gas, and assumes that field loss due to reconnection or magnetic diffusion is unimportant. Ionization in this scenario can be maintained by a combination of X-ray and energetic particle radiation expected from stars with strong magnetic fields, and possibly by the decay of short-lived radioactive species thought to be abundant in massive star forming regions (Diehl et al. 2004, 2006a, b).

Gas tends to be removed from the region occupied by compact multiple star systems by accretion onto individual circumstellar disks or expulsion by gravitational torques (Lubow & Artymowicz 1996). The removal of gas from the intermediate region with a characteristic length-scale comparable to the average interstellar separation implies that this region will have a large Alfvén speed. For a field strength of 40 gauss, the Alfvén speed exceeds 10^3 km s^{-1} for a density less than $1.3 \times 10^{-14} \text{ g cm}^{-3}$ ($n_H < 6 \times 10^9 \text{ cm}^{-3}$).

The momentum in the BN/KL outflow (Snell et al. 1983) is about $P_{out} = 160 \text{ M km s}^{-1}$. The momentum delivered by the ‘magnetic bomb’ to the sur-

rounding gas, $P_{MB} = M_{gas}V_A$, must therefore be at least this large. Consequently, the gas mass in the magnetized region must satisfy $M_{gas} > 3P_o^2ut/B^2r^3 \approx 0.3 M_\odot$ for $B = 40$ gauss and $r = 100$ AU. These parameters imply an average Alfvén speed of about 600 km s^{-1} , somewhat greater than the velocity of the very fastest knots in the outflow.

The strongest fields are likely to be generated by shear dynamos in the innermost parts of circumstellar disks surrounding individual massive stars. Thus, the highest velocity ejecta observed in the BN/KL outflow may have been launched by the dynamical disruption of highly magnetized material from within a few to tens of AU of the individual stars by the penetrating encounter that disrupted the star system. Reconnection of magnetic fields, steep magnetic pressure gradients, and centrifugal acceleration may also have contributed to the acceleration of the fastest ejecta. Fast ejecta slamming into slower material farther out can produce high velocity bullets and fingers (McCaughrean & Mac Low 1997; Stone, Xu, & Mundy 1995). Highly perturbed circumstellar disks with radii of at least several AU may survive the dynamical interactions and may be dragged along by the ejected stars. These remnant disks may continue to fuel collimated outflow activity along axes that reflect the changed disk orientations.

In summary, we propose that the Orion BN/KL outflow was powered by magnetic energy generated by the orbital motion of a non-hierarchical multiple stars system of 4 or more stars over 10^4 to 10^5 years, and released by dynamical decay a mere 500 years ago. This event led either to the formation of one or more compact binaries or possibly a stellar merger. A testable prediction of this scenario is that the Galaxy should contain a population of compact, massive, magnetized hot cores with field strengths of order 10 to 100 Gauss. Future interferometric observations of Zeeman splitting of far-infrared, sub-millimeter, or millimeter spectral lines should detect these magnetic fields on 100 AU length scales.

Acknowledgments. This work was supported by NSF grant AST0407356 and the CU Center for Astrobiology funded by NASA under Cooperative Agreement no. NNA04CC11A issued by the Office of Space Science.

References

- Allen, D.A., & Burton, M.G. 1993, *Nature*, 363, 54
- Bally, J., & Lane, A. P. 1990, in ASP Conference Series 14: *Astrophysics with Infrared Arrays*, ed. R. Elston, 273278
- Bally, J., & Zinnecker, H. 2005, *AJ*, 129, 2281
- Bally, J., Licht, D., Smith, N., & Walawender, J. 2006, *AJ*, 131, 473
- Bartkiewicz, A., Szymczak, M., Cohen, R. & Richards, A.M.S. 2005, *MNRAS*, 361, 623
- Beuther, H., Schilke, P., Gueth, F., McCaughrean, M., Andersen, M., Sridharan, T. K., & Menten, K. M. 2002, *A&A*, 387, 931
- Beuther, H. & Shepherd, D. S. 2005, in *Cores to Clusters: Star Formation with Next Generation Telescopes*, p. 105, M. S. N. Kumar et al. eds.
- Blaauw, A., Hiltner, W. A., & Johnson, H. L. 1959, *ApJ*, 130, 69
- Cohen, R.J., Gasprong, N., Meaburn, J., & Graham, M.F. 2006, *MNRAS*, 367, 541
- Cohen, R. J., Rowland, P. R., & Blair, M. M. 1984, *MNRAS*, 210, 425
- Crawford, D. L., & Barnes, J. V. 1970, *AJ*, 75, 952
- Cunningham, N. 2006, PhD Thesis, University of Colorado., Boulder
- Cunningham, N., Moeckel, N., & Bally, J. 2008, (in preparation)

- Diehl, R., Cervino, M., Hartmann, D. H. & Kretschmer, K. 2004, *New Astronomy Reviews*, 48, 81
- Diehl, R. et al. 2006, *A&A*, 449, 1025
- Diehl, R. et al. 2006, *Nature* 439, 45
- Doi, T., O'Dell, C.R., & Hartigan, P. 2002, *AJ*, 124, 445
- Garay, G., Ramirez, S., Rodríguez, L. F., Curiel, S., & Torrelles, J. M. 1996, *ApJ*, 459, 193
- Gezari, D. Y., Backman, D. E., & Werner, M. W. 1998, *ApJ*, 509, 283
- Genzel, R., Reid, M.J., Moran, J.M., & Downes, D. 1981, *ApJ*, 244, 884
- Gomez, L., Rodriguez, L.F., Loinard, L., Lizano, S., Poveda, A., & Allen, C. 2005, *ApJ*, 635, 1166
- Greenhill, L.J., Gwinn, C.R., Schwartz, C., Moran, J.M., & Diamond, P.J. 1998, *Nature*, 396, 650
- Gutermuth, R., Megeath, S. T., Pipher, J. L., Allen, L. E., Myers, P. C., & Fazio, G. 2005, in *Star Formation in the Era of Three Great Observatories*
- Hartigan, P., Lada, C. J., Tapia, S., & Stocke, J. 1986, *AJ*, 92, 1155
- Hartigan, P., Morse, J., & Bally, J. 2000, *AJ*, 120, 1436
- Hiriart, D., Salas, L., & Cruz-González, I. 2004, *AJ*, 128, 2917
- Hirota, T., et al. 2007, *ArXiv e-prints*, 705, arXiv:0705.3792
- Hughes, V. A., & Wouterloot, J. G. A. 1984, *ApJ*, 276, 204
- Kaifu, N., et al. 2000, *PASJ*, 52, 1
- Koppelaar, K., van Duinen, R. J., Aalders, J. W. G., Sargent, A. I., & Nordh, L. 1979, *A&A*, 75, L1
- Kwan, J., & Scoville, N.Z. 1976, *ApJ*, 210, L39
- Lubow, S. H. & Artymowicz, P. 1996, *ApJL*, 467, 77
- Lynden-Bell, D. 1996, *MNRAS*, 279, 389
- Matt, S., Frank, A., & Blackman, E. G. 2004, *The Last Hurrah: PPN Formation by a Magnetic Explosion*. ASP Conf. Ser. 313: Asymmetrical Planetary Nebulae III: Winds, Structure, and the Thunderbird, 313, 449
- Matt, S., Frank, A., & Blackman, E. G. 2006, *ApJ*, 647, L45
- McCaughrean, M.J., & Mac Low, M. 1997, *AJ*, 113, 391
- Menten, K. M., Reid, M. J., Forbrich, J., & Brunthaler, A. 2007, *A&A*, 474, 515
- Moeckel, N., & Bally, J. 2007, *ApJ*, 661, L183
- Moeckel, N., & Bally, J. 2007, *ApJ*, 656, 275
- Moeckel, N., & Bally, J. 2006, *ApJ*, 653, 437
- Narayanan, G., & Walker, C. K. 1996, *ApJ*, 466, 844
- Reipurth B. & Bally J. 2001, *Ann. Rev. Astron. Astrophys.*, 39, 403
- Reipurth, B., Jewitt, D., & Keil, K. 2007, *Protostars and Planets V.*, University of Arizona Press, Tucson
- Rodríguez, L. F., Ho, P. T. P., & Moran, J. M. 1980, *ApJ*, 240, L149
- Rodríguez, L.F., Poveda, A., Lizano, S., & Allen, C. 2005, *ApJ*, 627, L65
- Russell, A. P. G., Bally, J., Padman, R., & Hills, R. E. 1992, *ApJ*, 387, 219
- Sandstrom, K. M., Peek, J. E. G., Bower, G. C., Bolatto, A. D., & Plambeck, R. L. 2007, *ApJ*, 667, 1161
- Sargent, A. I. 1977, *ApJ*, 218, 736
- Sargent, A. I. 1979, *ApJ*, 233, 163
- Snell, R. L., Scoville, N. Z., Sanders, D. B., & Erickson, N. R. 1983, *ApJ*, 284, 176
- Sterzik, M. F. & Durisen, R. H., 1998, *A&A*, 339, 95
- Stone, J.M., Xu, J., & Mundy, L.G. 1995, *Nature*, 377, 315
- Torrelles, J. M., Verdes-Montenegro, L., Ho, P. T. P., Rodríguez, L. F., & Canto, J. 1993, *ApJ*, 410, 202
- Vlemmings, W.H.T., Diamond, P.J., van Langevelde, H.J. & Torrelles, J.M. 2006, *A&A*, 448, 597
- Wheeler, J.C., Meier, D.L., & Wilson, J.R. 2002, *ApJ*, 568, 807
- Wiseman, J.J., & Ho, P.T.P. 1996, *Nature*, 382, 139